Investigation of the Physical Aspects of Beta Imaging Probes Using Scintillating Fibers and Visible Light Photon Counters

L.R. MacDonald, M.P. Tornai*, C.S. Levin*, J. Park,
M. Atac, D.B. Cline & E.J. Hoffman*

Department of Physics
*Department of Pharmacology and Crump Institute for Biological Imaging
University of California, Los Angeles

Abstract

We are developing a hand held imaging probe intended for intra-operative use. This probe is to be used after the bulk of tumor has been removed. It will locate residual malignant tissue labeled by a pre-operative injection of a tumor seeking radiopharmaceutical. The device presented here is a prototype system that consists of a 4 x 8 array of 925μm diameter plastic scintillating fibers. The imaging array is coupled to Visible Light Photon Counters (VLPCs) via 2 meters of optical fiber. We have obtained an intrinsic spatial resolution of 1.0 mm with a highly collimated beta source, and a 2.0 mm resolution with a 1 mm, uncollimated source. Standard deviations of the relative gain and sensitivity over the 32 imaging elements were found to be 9.6% and 11.7% of the mean, respectively.

I. INTRODUCTION

The primary mass of a brain tumor is readily identified during surgery, but the boundaries, small extensions into normal tissue and small pieces of isolated tumor are difficult to determine precisely. The removal of residual tumor is very important to the recovery of the patient as even small amounts of tumor can lead to rapid reoccurrence of the disease[1-2]. It is equally important to avoid removing excess tissue that may be supporting vital functions. The current technique of multiple biopsies during surgery is time consuming and generally under-samples the tissue bed.

We are developing a hand held, imaging scintillation camera (imaging probe) to be used during surgery. The design goal is an imaging device that covers an area on the order of 1-2 cm^2 with intrinsic spatial resolution of the order of 1 mm. The probe will image distributions of radiopharmaceuticals that infiltrate the tumor at a significantly higher fraction than normal tissue. A promising candidate is ^{18}F-fluorodeoxyuridine (FDUR) which is reported to have a high tumor to tissue ratio [3-6]. This particular radiopharmaceutical allows diagnosis with PET to verify the location of the tumor and uptake of the FDUR. Then, during surgery, the imaging probe detects the positrons themselves instead of the 511 keV annihilation photons. This requires a detection system that is transparent to gamma radiation while remaining sensitive to betas.

II. PROTOTYPE IMAGING PROBE SYSTEM

A diagram of the system utilized for the measurements in this work is shown in Fig 1. Plastic scintillating fibers form the detector array, which are then coupled to clear optical fibers which are in turn coupled to Visible Light Photon Counters, or VLPCs.

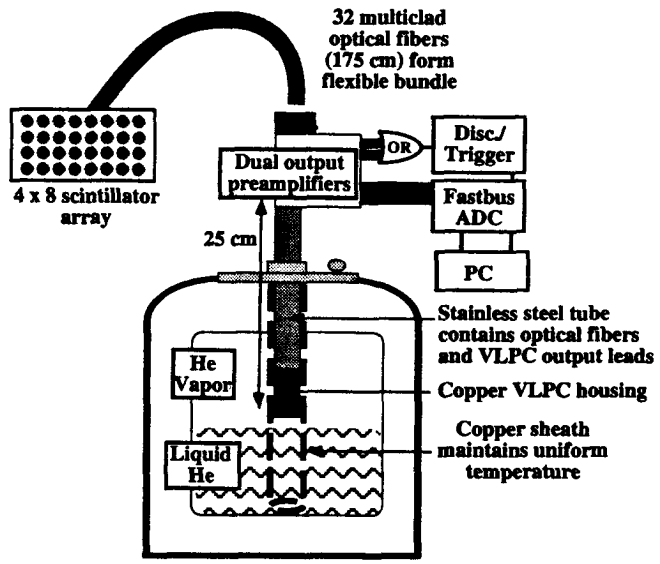

Figure 1. Components of the beta imaging intra-operative probe. A small liquid helium dewar is used to cool VLPCs which operate at about 7 degrees K in the vapor above the liquid.

A. Scintillating and Optical Fibers

The fiber optic bundle allows the concept to work by providing a light, flexible signal path to the relatively bulky VLPC dewar and electronics cabinet. The fiber optic bundle also creates one of the major challenges of the technique since one expects only about 2-4% of the photons produced in the scintillator to reach the other end of the fiber optic. The bundle provides a minimum of 2 meters of insulation from any source of high voltage, which is always a concern with patient involvement. The patient end of the fiber optic bundle is an optical coupler, which will allow a number of different

0-7803-2544-3/95 $4.00 © 1995 IEEE

The choice of lower channel in the Gaussian fit method was more ambiguous. The only part of the gamma spectra that might be expected to have a Gaussian shape is the usually sharp Compton edge that will smear because of the poor photon statistics of the system, forming an asymmetric, semi-Gaussian shape. This analysis was very sensitive to the low channel chosen and to variations among the 32 individual imaging elements of the probe.

B. Beta Spectra

A traditional way of analyzing beta spectra is via a graph known as a Kurie plot. A simple manipulation of the complicated equation for the theoretical beta energy distribution leads to a new expression that, when plotted versus energy, gives a straight line from which the maximum energy of the spectrum can be extracted [14-15].

The problems encountered with this technique were rooted in its reliance on the analytical expression for the spectral shape. Deviations from the theoretical spectral shape cause distortions in the Kurie plot, complicating this analysis. Distortions can result from a number of factors: 1) contamination from 511 keV annihilation gammas; 2) the small size of the scintillators may result in incomplete energy deposition; 3) absorption of positrons in surrounding material.

The weighted mean technique outlined in section III A. is also applicable to the beta spectrum.

IV. CALIBRATION

A. Gain and Sensitivity

The result of the gain and sensitivity calibrations using the methods described above can be seen in Figure 3. Both Kurie plot and weighted mean methods were used to calculate the gain variations for a ^{204}Tl flood irradiation. In Fig. 3a. these two measurements are normalized to one another. Weighted mean analysis of gamma sources (^{57}Co, ^{131}I, ^{68}Ge-Ga, ^{137}Cs and ^{60}Co) showed similar variations. The Kurie plot method yielded the smallest standard deviation, 9.6% of the mean. The weighted mean technique gave similar results; standard deviations ranged from 9%-12%.

To measure the sensitivity variation we corrected the sensitivity calculations by the gain variations found in Fig. 3a. The gain corrected sensitivity is displayed in Fig 3b.

B. Energy Calibration

Spectral analysis techniques of sect. III A were used to calculate the relationship between source energy and Fastbus ADC channel. Ideally, this relationship would be linear, but because of the small size of the scintillators, non-linearity was anticipated and found. A monotonic increase in ADC channel was seen with increasing source energy, but consistently leveled off at higher energies.

C. Monte Carlo Simulations

To understand the energy calibration result, we used Monte Carlo simulations to model beta and gamma interaction in the scintillators. The Monte Carlo code EGS4 was used to model energy deposition of various sources in the scintillators.

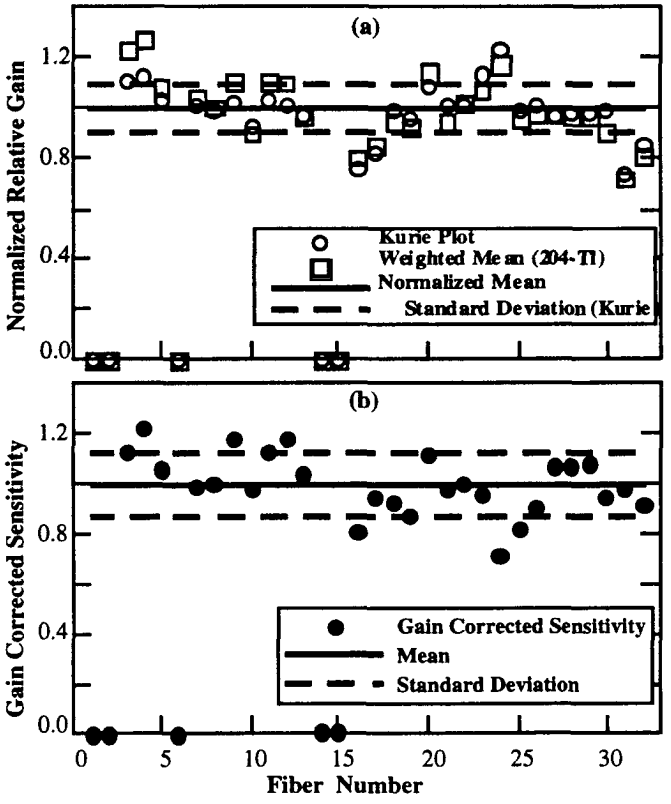

Figure 3. (a) Gain variation of the 32 element probe. Normalized results from both Kurie plot and weighted mean analyses for ^{204}Tl are seen. (b) Gain corrected sensitivities of the individual fiber elements. Five dead channels are seen on the x-axes.

The Monte Carlo showed the scintillators to absorb energy from only 13%-18% of the incident gammas, depending on source energy. The simulated beta source (^{204}Tl) showed energy deposition for 80% of the events. Energy deposition simulated for small scintillators did show a defined Compton edge for low energy sources (Fig. 4a). The Compton electrons can scatter without full energy deposition, but because of the length of the scintillators (2.5 cm), electrons from photon scattering near 180^{o} can be fully absorbed, producing a sharp Compton edge. However, at the energy of ^{60}Co (gammas at 1173 & 1332 keV) the Compton edge disappears. The typical plateau region below the Compton edge is not seen in Fig. 4a, as the finite resolution of the system blurs the spectrum it becomes difficult to identify the location of the Compton edge (as in Fig. 2).

An intrinsic resolution was added to the simulated spectrum. Physically, this resolution can be attributed to variation in the scintillator's conversion efficiency, the ability of the scintillation photons to escape the scintillating fibers,

imaging probes with specialized geometries to be exchanged during surgery.

The scintillating and clear fibers are of the multiclad type (Kurrary Corp.) in which the outermost cladding is made of a fluorinated polymer with an index of refraction (n) equal to 1.42. The second cladding is polymethylmethacrylate (PMMA) with n = 1.49, and the core is polystyrene with n=1.59. The large difference in the n values of the outer clad and the core maximizes the amount of light trapped in the fiber, and the outer clad also acts as a protective coating, preventing surface imperfections and damage to the inner clad. The multiclad fibers have an 825 μm diameter core and two 25 μm thick claddings

The imaging array of scintillators employed in this test system consists of a 4 by 8 set of 0.15% 3-hydroxyflavone (3HF) doped multiclad fibers. The 3HF fluorescence emission peaks near 535 nm. In a low density material such as polystyrene, positrons are readily absorbed, and the absorption of energy from 511 keV gammas is minimal. The scintillators are 2.5 cm long and the fiber centers are spaced by 1.27 mm. Each is thermally fused [7-8] to a 175 cm long, multi-clad, clear fiber. The attenuation length in the clear fibers is 7 - 8 m at 503 nm [9]. 32 of the clear fibers form a bundle that is then coupled to a 25 cm long set of fibers that extend to VLPCs (Fig 1). The experimental setup was fabricated from materials at hand, and are not the result of any attempt to build an optimized system. We are in the process of optimizing the system, first by Monte Carlo simulation, which will guide our initial attempts at optimized designs.

B. VLPCs

The photo detectors used were the latest version of VLPCs, designated HISTE-IV (Rockwell International Science Center) [9-12]. VLPCs are silicon based solid state photon detectors with unusually high quantum efficiency. At the wavelength of 3HF the quantum efficiency is between 60-70%. The VLPCs have a fast rise time (< 10 ns), operate continuously, have low power requirements (~1μW, - 6.5 V operating voltage) and a gain of over 10^4. To achieve this sensitivity thermal noise must be suppressed by cooling to 7 degrees K. This is accomplished by operating the VLPCs in the vapor of a liquid helium dewar (Fig. 1).

Special cryostat cold-finger cassettes house the VLPCs. In our cassette, 4 linear arrays of 8 VLPCs, 1 mm in diameter each, are mounted in the cold-finger that will be inserted into a super-insulating dewar containing liquid helium. Fiber optics (sect. II B) lead from the top of the cassette and are epoxied in position about 75μm from the surface of the VLPCs. Repeated tests have shown that thermal cycling of these fibers causes no ill effects. Fine leads carry the VLPC signal up and out of the cold-finger where connections to preamplifiers are made.

C. Data Acquisition Hardware

The VLPC signals are fed into fast, transimpedance preamplifiers (QPA02, [13]). The preamps have two output signals; one set goes to an analog OR circuit with the output delivered to a NIM discriminator. The discriminator supplies a trigger to a Fastbus ADC (LeCroy model 1885F) where the other set of preamp outputs is digitized (Fig. 1). The Fastbus is controlled with Lift3 software (LeCroy) on a PC.

III. SPECTRAL ANALYSIS

One of the difficulties in characterizing the imaging probe is the establishment of an energy calibration to allow a valid normalization of the sensitivity of each element. The energy spectrum of a beta emitter is a continuum, therefore, there is no photopeak for setting up an energy window as with most gamma imaging devices in nuclear medicine.

A. Gamma Spectra

The probe is specifically designed to be insensitive to gamma rays, and attempting to detect even the Compton edge of several gamma sources for purposes of calibration proved difficult. A clear Compton edge was never seen and the resulting spectra were continua with few features. Figure 2 is a set of four spectra acquired with one of the probe's 32 fiber elements.

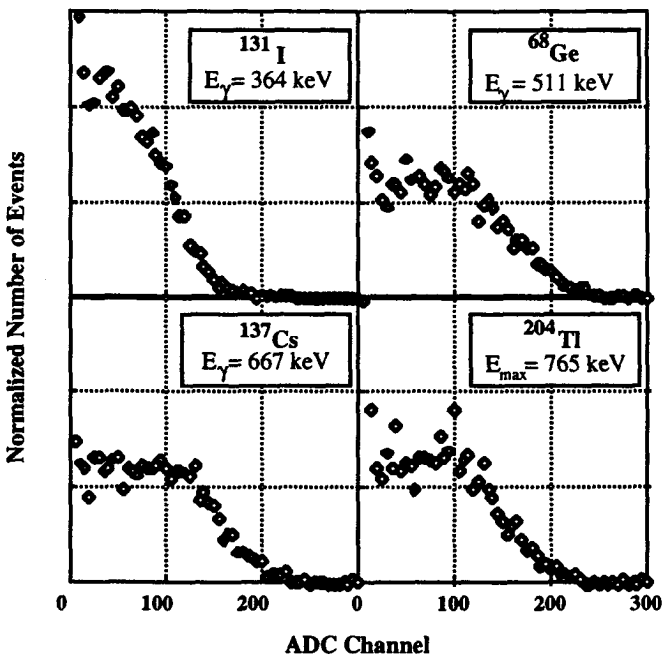

Figure 2. Spectra of 3 gamma sources and a beta source (^{204}Tl) acquired with channel 11 of the prototype beta-imaging intra-operative probe.

We analyzed the gamma spectra in two ways: (1) Fit the region of the "Compton edges" to a Gaussian and compare centroids of different energy sources. (2) Calculate weighted means of the spectra. The weighted mean calculation used the entire spectrum, excluding only electronic noise.

statistical variances in the coupling and attenuation losses and slight VLPC variability. Rough estimations, previous experience with this type of system and parameters and trial and error led to an estimated resolution of 20% and a 50 keV threshold for the simulated spectra.

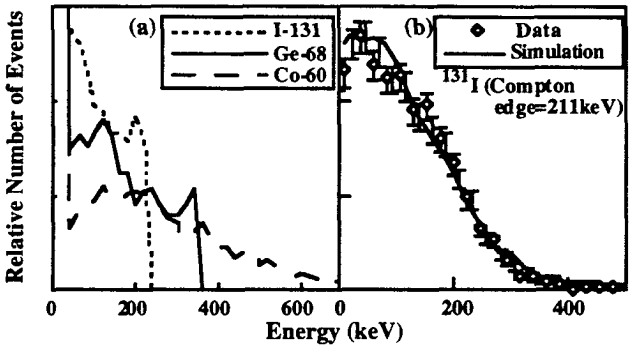

Figure 4. (a) Simulated energy deposition from the indicated sources in the scintillating fibers of the probe, i.e. the best spectra the probe could produce. No light transport is included here. Compton edges are visible for the lower energy sources, but not for ^{60}Co which emits gammas at 1170 & 1330 keV. (b) Simulation of a realistic detector system with finite resolution compared to acquired data spectrum.

Fig. 4b shows an example of a comparison between acquired data and a simulated spectrum. The simulation can be a useful guide in studies to optimize the scintillator geometry for energy deposition and background minimization. We are beginning to concentrate on the testing and calibration of modified systems.

IV. SPATIAL RESOLUTION

Spatial resolution was measured with collimated ^{204}Tl beta sources. The scintillating fibers should have a higher sensitivity to beta particles and they are easier to collimate.

Point spread functions of the probe are shown in Fig. 5. This measurement was made with a 0.5 mm line source scanned across the scintillating array. Fig. 5 shows one of the rows of scintillators after correction for gain and sensitivity. The central six fibers are displayed. Individual peaks are fit to Gaussians, the mean full width half maximum is 1.03 ± 0.05 mm and the mean spacing between centroids is 1.26 ± 0.07 mm.

Two different source configurations were utilized to measure the performance of the probe's spatial resolution. One is a 1.0 mm diameter pencil beam of forward directed betas. The other is a source 1 mm in extent but uncollimated, thus betas are emerging in a 2π solid angle. With the pencil beam we can consistently detect a signal in exclusively one of the 32 scintillators. The response of the probe to these two source arrangements is shown in Fig. 6, where each lego represents one of the scintillating fibers.

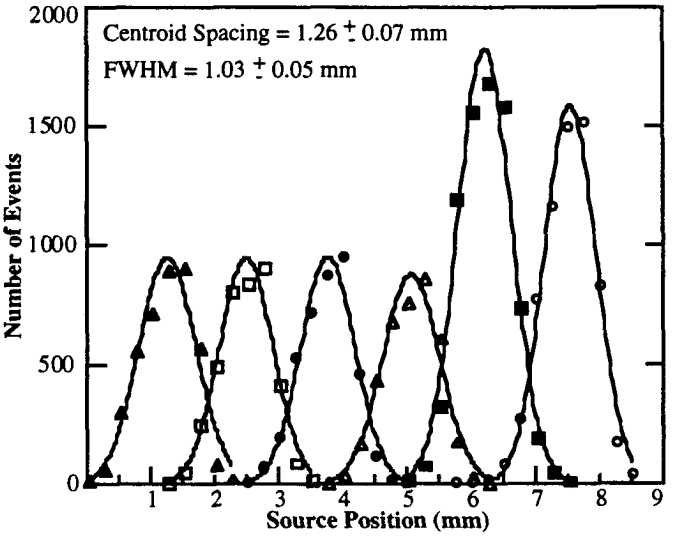

Figure 5. Point spread function of probe. Mean FWHM and centroid spacing are indicated. Error bars on these data are the size of the data points.

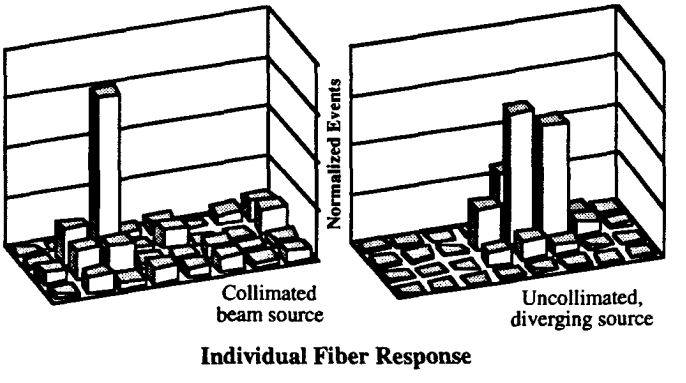

Figure 6. Probe response to collimated and diverging 1 mm beta sources. 925 μm diameter fibers, center spaced 1.27 mm, are represented by square pixels here. Dead space is depicted.

The dead space of this design (packing fraction of 0.56) called for an over sampling of the active source area. To do this we acquired data in four positions to create a single image. The four positions formed a square and were separated by one half the center to center fiber spacing. By moving the probe one half pixel steps we fill the dead space area. This technique was applied to the same sources used in Fig. 6. Fig. 7 shows the resulting finer resolution of this method.

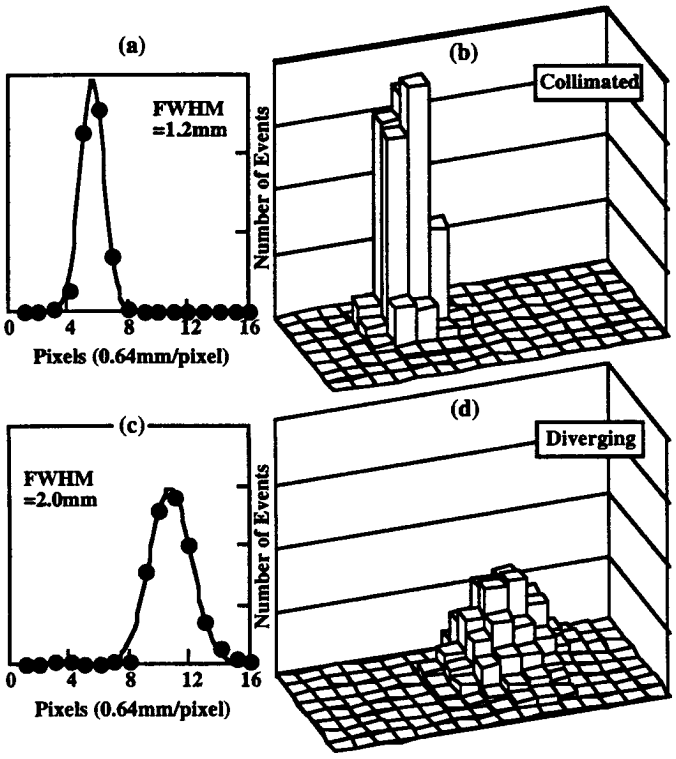

Figure 7. Interleaving technique fills dead space. The same sources as Fig. 6 are more finely sampled. In (b) & (d) the number of events are normalized and 4 boxes are equivalent to one fiber of the probe. In (a) & (c) cuts from (b) & (d), respectively, are fit to Gaussians. Full width half maximum are given.

V. CONCLUSION

Our preliminary investigation of the physical aspects of a beta imaging probe has resulted in promising performance possibilities. The availability of the VLPCs has allowed the long optical fiber bundle to be utilized while maintaining usable signals with energy sensitivity.

We have demonstrated that millimeter spatial resolution is achievable with a small array of scintillators and that source distributions distinguish themselves. Despite non-optimal scintillator geometry an energy calibration trend was observed. Energy spectra are pronounced enough that reasonable gain and sensitivity corrections can be made.

VI. ACKNOWLEDGMENTS

The authors thank Claudio H. Rivetta of FERMILAB for technical assistance.

This work was funded in part by DOE Contract DE-FC03-87-ER60615 and NCI grant R01-CA61037.

VII. REFERENCES

[1] P. Black and S. Ronner, "Cortical Mapping for Defining the Limits of Tumor Resection", Neurosurgery, vol. 20, No. 6, pp. 914-919, 1987

[2] P. Black, "I. Brain Tumors, Medical Progress-Review Article", New Eng J Med, vol. 324, No. 21, pp.1471-1476

[3] Y. Abe *et al.*, "Tumor Uptakes of ^{18}F-5-Fluorouracil, ^{18}F-5-Fluorouridine, ^{18}F-5-Fluorodeoxyuridine in Animals", Eur J Nuc Med, vol. 8, pp.258-261, 1983

[4] K. Ishiwata *et al.*, "II. Metabolic Investigation of ^{18}F-5-Fluorouracil, ^{18}F-5-Fluoro-2'-deoxyuridine and ^{18}F-5-Fluorouridine in Rats", Eur J Nuc Med, vol. 9, pp.185-189, 1984

[5] K. Ishiwata *et al.*, "Metabolic fates of ^{18}F-5-Fluoro-2'-deoxyuridine in Tumor Bearing Mice and Human Plasma", Nuc Med Biol, 18: pp. 539-545, 1991

[6] S. Starosta-Rubinstein *et al.*, "Imaging of a Glioma Using Peripheral Benzodiazepine Receptor Ligands", Proc Natl Acad Sci USA, vol. 84, pp. 891-895, 1987

[7] M.Atac, W.Foster and M. Lundin, Fermilab Pub-537, 1990

[8] G. Apollinari, D. Scepanovic and S. White, "Plastic Optical Fiber Splicing by Thermal Fusion", NIM A311, pp.520-528, 1992

[9] B. Baumbaugh *et al.*, NIM A345, pp. 271-278, 1994

[10] M.D. Petroff and M.G. Stapelbroek, IEEE Trans. Nucl. Sci. NS-36 (1) pp.158-162, 1989

[11] M.D. Petroff and M. Atac, IEEE Trans. Nucl. Sci. NS-36 (1), pp. 163, 1989

[12] M. Atac *et al.*, "Scintillating Fiber Tracking for the SSC Using Visible Light Photon Counters", NIM A314, No. 1, pp. 56-62, 1992

[13] T. Zimmerman, "A High Speed, Low Noise ASIC Preamplifier for Silicon Strip Detectors", IEEE Trans. Nucl Sci NS-37 (2), pp. 439-443, 1990

[14] H. Daniel, "Shapes of Beta-Ray Spectra", Rev Mod Phys, vol. 40, pp.659-672, 1968

[15] I. Feister, "Numerical Evaluation of the Femi Beta-Distribution Function", Rev Mod Phys, vol. 78, pp.375-377, 1950